Proceedings of the 9th U.S. National and 10th Canadian Conference on Earthquake Engineering
Compte Rendu de la 9ième Conférence Nationale Américaine et
10ième Conférence Canadienne de Génie Parasismique
July 25-29, 2010, Toronto, Ontario, Canada • Paper No 1330

SEISMIC PERFORMANCE OF A SELF-CENTERING ROCKING CONCENTRICALLY-BRACED FRAME

R. Sause[1], J.M. Ricles[2], D.A. Roke[3], N.B. Chancellor[3], and N.P. Gonner[4]

ABSTRACT

Conventional concentrically-braced frame (CBF) systems have limited drift capacity before brace buckling and related damage leads to deterioration in strength and stiffness. A new type of CBF is being developed which has greater drift capacity before damage and which develops much less permanent (residual) drift under seismic loading. This self-centering CBF (SC-CBF) system is motivated by the goal of minimizing structural damage under seismic loading and is intended to provide significant non-linear drift capacity while limiting damage and residual drift. The fundamental lateral load behavior of the SC-CBF system is rocking on its base, which occurs when the column under tension from overturning moment decompresses and uplifts from its support. The SC-CBF is designed to decompress at the base at a selected level of lateral loading, initiating a rigid-body rotation (rocking) of the frame. Vertically-aligned post-tensioning (PT) steel resists this uplift and provides a restoring force to return the SC-CBF to its support (to re-center the system). Experimental and analytical results show that SC-CBFs can be designed to sustain no significant structural damage under the design basis earthquake and only minor structural damage under the maximum considered earthquake.

Introduction

Steel concentrically-braced frame (CBF) systems are stiff and economical earthquake-resistant steel frame systems, which often exhibit limited system ductility capacity. The ductility capacity can be increased using buckling-restrained braces (e.g., Fahnestock et al. 2003); however, the buckling-restrained braced frame (BRBF) system sometimes exhibits significant residual drift after an earthquake. To increase the ductility and reduce the residual drift of CBFs, the self-centering concentrically-braced frame (SC-CBF) systems is being developed.

Recent research on self-centering (SC) unbonded post-tensioned (PT) precast wall

[1]Joseph T. Stuart Professor of Structural Engineering, ATLSS Center, Dept. of Civil and Environmental Engineering, Lehigh University, Bethlehem, PA 18015
[2]Bruce G. Johnston Professor of Structural Engineering, ATLSS Center, Dept. of Civil and Environmental Engineering, Lehigh University, Bethlehem, PA 18015
[3]Graduate Research Assistant, ATLSS Center, Dept. of Civil and Environmental Engineering, Lehigh University, Bethlehem, PA 18015
[4]Structural Designer, Skidmore, Owings, and Merrill

systems (e.g., Kurama et al. 2002) and on SC steel moment-resisting frames with PT connections (e.g., Ricles et al. 2001, 2002) suggests that self-centering system concepts can be applied to CBFs (Roke et al. 2006). This paper summarizes design concepts and criteria for SC-CBF systems, and summarizes the seismic performance of an SC-CBF test structure.

System Behavior

The SC-CBF system and its idealized behavior are shown schematically in Fig. 1. The system consists of beams, columns, and braces in a conventional arrangement (Fig. 1(a)), with column base details that permit the columns to uplift at the foundation (Fig. 1(c)). Gravity loads and post-tensioning (PT) forces (from PT steel arranged along the column lines in the system shown in Fig. 1(a)) resist column uplift and provide a restoring force after uplift. The beams, columns, and braces are intended to remain essentially elastic under the design earthquake, and the column uplift provides a mechanism for controlling the force levels that develop in the frame under earthquake loading.

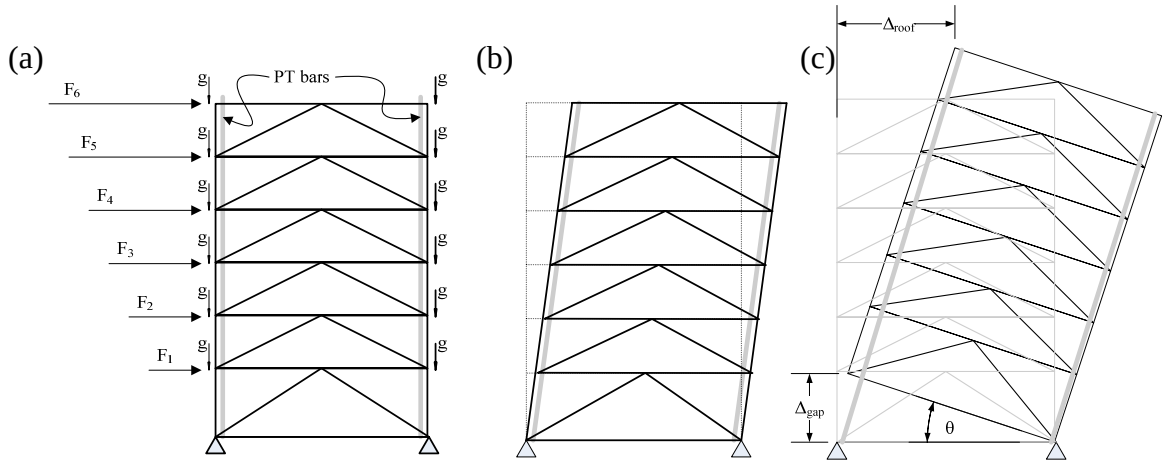

Figure 1. SC-CBF system: (a) schematic of members and loads; (b) elastic response prior to column decompression and uplift; (c) rigid-body rotation after column decompression and uplift.

Fig. 1(a) shows loads used in a lateral force seismic analysis of an SC-CBF. Gravity loads (g) are applied at the columns at each floor level. The lateral load profile (F_i) is similar to that used in an equivalent lateral force procedure (ICC 2003). Under low levels of lateral force, the structure deforms elastically as shown schematically in Fig. 1(b). This deformation is similar to that of a conventional CBF. Under higher levels of lateral force, the overturning moment at the base of the frame becomes large enough for the "tension" column to decompress, and uplift of the column occurs, as shown in Fig. 1(c). After column decompression and uplift, the lateral displacement of the frame is dominated by rigid body rotation of the SC-CBF about the base of the "compression" column (i.e., frame rocking), although some additional forces and deformations develop in the beams, columns, and braces of the frame. The PT steel elongates from the uplift of the frame, leading to an increase in PT force, which provides a positive stiffness to the lateral force-lateral drift behavior after column decompression and uplift.

Frame Configuration

Several SC-CBF configurations have been studied (Roke et al. 2006, 2009). Frame D_{DIST}, was selected for detailed study. This configuration, shown in Fig. 2, consists of an SC-CBF placed between two additional columns that are attached to the gravity load system of the building. These two "gravity columns," which do not uplift, separate the gravity load carrying function from the rocking of the SC-CBF. "Friction-bearing" dampers are located so that slip can occur due to the relative vertical displacement between the gravity columns and the SC-CBF columns. Each friction-bearing damper has a small initial gap between the gravity column and SC-CBF column, which is closed by the transfer of floor diaphragm inertial forces in bearing between the gravity column and the SC-CBF column. The normal force on the friction surface equals the floor diaphragm inertial force transferred to the SC-CBF at a floor level. The steel-on-brass friction surface has a friction coefficient of approximately 0.5. To reduce the elongation demand on the PT steel, the PT steel is located at midbay of the SC-CBF. As the tension column uplifts and a gap opens at the column base, the elongation demand on the PT steel is half of the gap-opening displacement of the uplifting column, Δ_{gap} (Fig. 1(c)). A vertical "distribution" strut is located in the upper story. This strut distributes the force of the midbay PT steel to the braces over multiple stories, thereby reducing the concentration of force in the braces in the upper story.

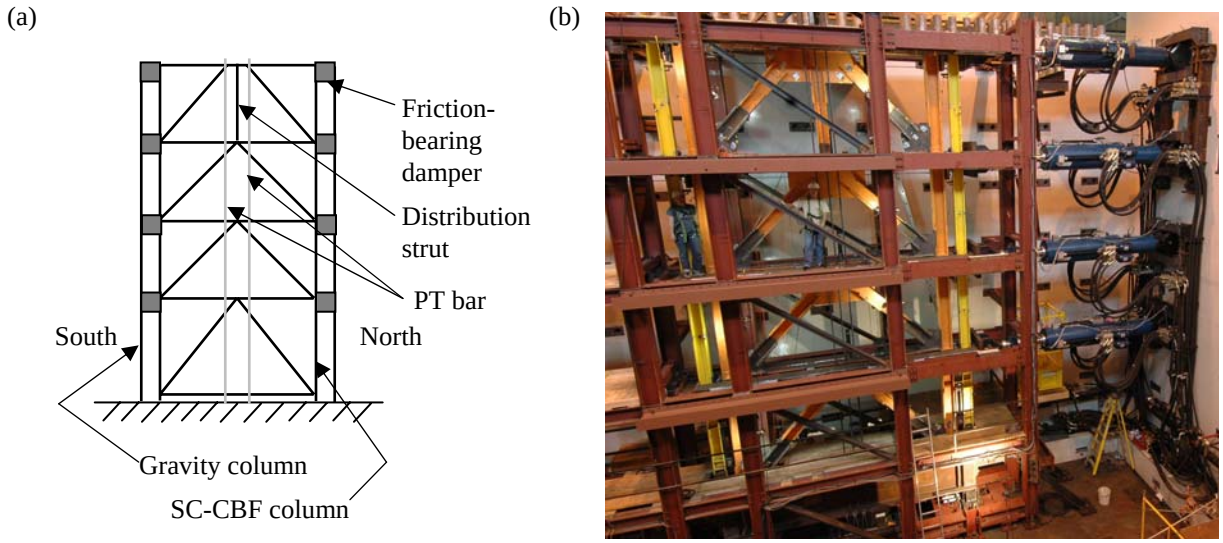

Figure 2. Frame configuration D_{DIST}: (a) schematic; (b) photo of test structure.

Limit States and Performance-Based Design

The primary limit states considered in the performance-based seismic design (PBD) of an SC-CBF are: (1) decompression and uplift of the "tension" column at the base of the SC-CBF; (2) yielding of the PT steel; (3) significant yielding of the beams, columns, or braces of the SC-CBF; and (4) failure of the beams, columns, or braces. Two seismic hazard (ground motion intensity) levels, as defined by FEMA 450 (BSSC 2003), are considered: (1) a design-basis earthquake (DBE) and (2) a maximum considered earthquake (MCE). The performance objectives are immediate occupancy (IO) under the DBE and collapse prevention (CP) under the

MCE. To reach these objectives, the four primary limit states are considered as follows (Fig. 3).

Decompression and uplift of the SC-CBF columns will not produce structural damage if the column bases and the attachment of the SC-CBF to the floor system are properly detailed, so this limit state conforms to the IO performance level. The prestress force in the PT steel is important to the self-centering behavior of SC-CBFs. Therefore, significant yielding of the PT steel, which produces a subsequent loss in prestress force (or fails the PT steel) could have serious consequences. Some types of PT steel and associated anchorage systems, for example, certain high strength PT bar systems, can yield and provide ductile behavior without immediate failure (Perez et al. 2003). However, other types of PT steel and associated anchorage systems, for example, certain high strength PT strand systems, may fail at the anchorages shortly after yielding. The SC-CBF system studied here employs high strength PT bars, and, therefore, the primary consequence of PT steel yielding is the subsequent loss of prestress force under cyclic loading. This loss of prestress is a form of structural damage that does not compromise the safety of the SC-CBF system, however, it must be repaired after an earthquake (by re-stressing or replacing the PT steel). Therefore, yielding of the PT steel is a limit state that conforms to the CP performance level, but not to the IO performance level (Fig. 3).

Significant yielding of the beams, columns, or braces of the SC-CBF is the initiation of significant structural damage to the SC-CBF system. To control the amount of damage that must be repaired after ground motions at an intensity level between the DBE and MCE levels, this limit state should be reached only after yielding of the PT steel (Fig. 3). Yielding of the PT steel provides a mechanism to control force levels in the SC-CBF, making it possible to control significant yielding of the other structural members. The PBD approach uses a capacity design method for the beams, columns, and braces of the SC-CBF to keep these members essentially elastic at seismic input levels that cause PT steel yielding. Failure (buckling or fracture) of the beams, columns, or braces of the SC-CBF is a limit state that may not conform to the CP performance level (Fig. 3). The force level control provided by yielding of the PT steel, as well as the inherent ductility of these steel members, are used to control this limit state.

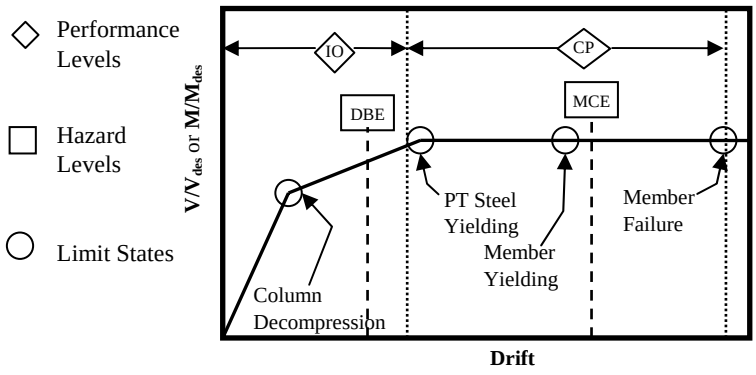

Figure 3. Summary of performance-based design criteria.

Test Structure Design Summary

A prototype structure was designed using the SC-CBF system. The prototype structure is

a four-story office building designed for a stiff soil site in Van Nuys, California. A 0.6-scale model of the prototype structure is shown schematically in Fig. 4, where SC-CBFs are shown located symmetrically throughout the plan. The test structure represents one SC-CBF with the adjacent gravity columns. Estimated gravity loads and seismic masses were determined using the following assumptions. The dead load includes the concrete floor slab, steel floor deck, mechanical equipment, floor and ceiling finishes, cladding weight, and an estimated weight per square foot of structural steel. The seismic mass of each floor is determined from the dead load plus the weight of interior partitions. The tributary seismic masses for the test structure, from the first floor to the roof, are: 135900 kg, 134800 kg, 134800 kg, and 142200 kg. The gravity loads carried by the associated $1/4^{th}$ of the gravity load bearing system of the building, from the first floor to the roof, are: 1495 kN, 1484 kN, 1484 kN, and 1556 kN.

The design of the SC-CBF system is based upon an equivalent lateral force (ELF) procedure (ICC 2003) modified to meet the performance-based design objectives described above. The initial value of the response modification factor, R, is 8. R is modified during the design process. The value of R is controlled by the design objective of avoiding PT steel yield under the DBE. The drift capacity at PT yield is controlled by rigid-body rotation (after column decompression) and elastic deformation of the SC-CBF up to PT yield. The rigid-body rotation elongates the PT steel, while the elastic deformation does not. The DBE drift demand equals the drift at decompression amplified by μ, which is calculated from μ-R relationships developed for self-centering systems (Seo 2005). As R decreases, μ decreases, and therefore, R is decreased in the design process until a sufficient margin of safety between the DBE drift demand and the drift demand at PT yield is provided.

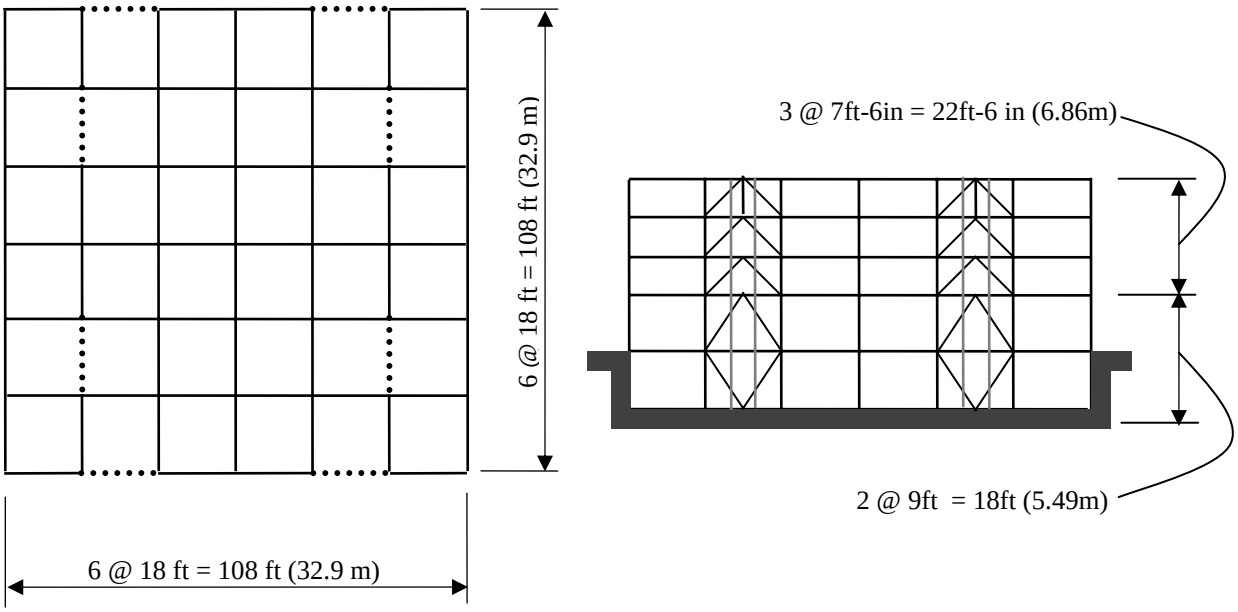

Figure 4. Prototype structure at 0.6 scale: (a) plan; (b) elevation of column line with SC-CBFs.

The SC-CBF beams, columns, and braces (members) are designed according to the PBD criteria discussed earlier. The member force demands were determined using a response spectrum procedure modified to meet the performance-based design objectives described above,

as discussed by Roke et al. (2009). The first mode demand is controlled by the overturning moment at the PT yield limit state. The higher mode demands are determined from a linear response spectrum analysis of the SC-CBF. The first mode and higher mode demands are then combined using the complete quadratic combination rule (Roke et al. 2009). The PT bars selected for the test structure are six 1 in (25.4 mm) nominal diameter PT bars, for a total PT bar area of 5.1 in^2 (3290 mm^2). The A992 steel sections selected for the test structure are W8x67 gravity columns; W10x112 frame columns; W12x50 beams; W8x48 first, second, and third story braces and distribution strut; and W8x58 fourth story braces.

To provide context for the SC-CBF test structure design, it was compared to the design of a special CBF (SCBF) and a BRBF. Table 1 summarizes R values for the SC-CBF test structure, the SCBF, and the BRBF. Other design quantities, such as the design base shear and design brace forces, are also compared. The design base shear, V_{bdes}, varies inversely with R. For the SCBF and the BRBF, the design brace force in each story (F_{b1des} through F_{b4des}) is estimated by assuming each brace in a story resists half of the story shear corresponding to the design lateral forces. The design brace forces are much higher for the SC-CBF system because the braces are specifically designed to account for higher mode response as described earlier. In addition, the design brace forces for the 3rd and 4th stories of the SC-CBF include the effects of the force in the midbay PT steel.

Table 1. Summary of design values (1k = 4.448kN).

System	R	V_{bdes} (k)	F_{b1des} (k)	F_{b2des} (k)	F_{b3des} (k)	F_{b4des} (k)	θ_r (%)
SC-CBF	7.8	155.7	384.9	231.7	376.0	479.1	1.1
SCBF	6	201.6	157.5	126.5	98.0	54.5	--
BRBF	8	151.2	118.1	94.9	73.5	40.8	--

Analytical and Laboratory Simulation Results

The seismic response of the SC-CBF test structure was characterized using nonlinear time history analyses performed using OpenSEES (Mazzoni 2006). A suite of 30 scaled DBE-level recorded ground motions and a suite of 30 scaled MCE-level recorded ground motions were used. The beams, columns, and braces of the SC-CBF were modeled as linear elastic so the member force demands required to keep the members linear elastic could be determined. The PT steel was modeled using nonlinear beam-column elements. The gap opening behavior and friction behavior at the column bases and at the friction-bearing dampers were modeled using contact friction elements. Rayleigh damping was used with 2% and 5% damping in the 1st and 3rd modes, respectively.

The response of the analytical model to the DBE and MCE records is summarized in Table 2. From the 30 DBE records and 30 MCE records, the ground motions shown in Table 2 were chosen to represent the mean, mean-minus-one-standard-deviation, and mean-plus-one-standard-deviation responses for each hazard level. Mean responses for the DBE and MCE are also presented in the table. The tabulated values are SF, the scale factor applied to each ground motion record; V_b/V_{bdes}, the maximum base shear demand normalized by the design base shear; F_{bi}/F_{bides}, the maximum brace force in story i normalized by the design brace force in story i; θ_r, the maximum roof drift; and θ_s, the maximum story drift from any story.

The test structure (Fig. 2 (b)) was subjected to numerous simulated earthquakes using the hybrid simulation method. During these laboratory simulations, a lateral force at each level was applied by hydraulic actuators through a floor diaphragm model consisting of a loading beam system attached to the both the north and south gravity columns shown in Fig. 2. This load was then transferred to the SC-CBF columns through the friction-bearing dampers described earlier. In the hybrid simulations, the test structure (SC-CBF and 2 adjacent gravity columns) is the experimental substructure, while the remaining gravity load bearing system, gravity loads, and seismic mass tributary to the test structure are included in the analytical substructure. The hybrid simulations used Rayleigh damping with 2% and 5% damping in the 1st and 3rd modes, respectively. Table 3 summarizes the experimental response of the test structure. Each response quantity is well-predicted by the analytical model. The correlation between the analytical response and the response from the laboratory simulations is illustrated in Figs. 4 through 7.

Table 2. Summary of analytical response.

Identifier	Input Level	SF	V_b/V_{bdes}	F_{b1}/F_{b1des}	F_{b2}/F_{b2des}	F_{b3}/F_{b3des}	F_{b4}/F_{b4des}	θ_r (%)	θ_s (%)
Mean	DBE	--	2.62	0.75	0.75	0.71	0.56	0.880	0.981
Mean	MCE	--	3.18	0.91	0.94	0.90	0.71	1.467	1.582
cls000	DBE	0.73	1.79	0.52	0.60	0.69	0.50	0.641	0.720
5108-090	DBE	2.49	2.85	0.82	0.75	0.86	0.60	0.827	0.909
h-shp270	DBE	1.75	3.01	0.86	0.85	0.82	0.65	0.912	1.023
arl090	DBE	1.40	2.92	0.84	0.79	0.87	0.69	1.389	1.521
stn110	MCE	1.98	2.91	0.84	0.90	1.06	0.78	1.622	1.747
a-tmz270	MCE	2.55	3.48	0.97	0.84	0.94	0.70	1.120	1.246
lp-hda255	MCE	2.24	3.38	0.95	1.04	0.91	0.74	1.477	1.588
nr-pel360	DBE	1.55	3.38	0.97	0.97	0.92	0.73	0.952	1.156
cap000	MCE	1.45	3.31	0.93	1.08	0.88	0.74	2.068	2.221
h-cpe237	MCE	3.85	3.70	1.07	0.97	0.89	0.71	1.741	1.831

Table 3. Summary of experimental response from laboratory simulations.

Identifier	Input Level	SF	V_b/V_{bdes}	F_{b1}/F_{b1des}	F_{b2}/F_{b2des}	F_{b3}/F_{b3des}	F_{b4}/F_{b4des}	θ_r (%)	θ_s (%)
cls000	DBE	0.73	1.92	0.54	0.61	0.64	0.49	0.650	0.760
5108-090	DBE	2.49	3.01	0.83	0.78	0.74	0.62	0.781	0.910
h-shp270	DBE	1.75	3.12	0.86	0.86	0.73	0.62	0.916	1.035
arl090	DBE	1.40	3.00	0.82	0.85	0.81	0.65	1.342	1.443
stn110	MCE	1.98	2.88	0.75	0.94	1.07	0.76	1.553	1.718
a-tmz270	MCE	2.55	2.93	0.80	0.84	0.88	0.67	1.120	1.234
lp-hda255	MCE	2.24	3.54	0.96	1.02	0.86	0.73	1.412	1.549
nr-pel360	DBE	1.55	3.35	0.87	0.83	0.78	0.66	0.982	1.134
cap000	MCE	1.45	3.43	0.88	1.09	0.82	0.68	1.872	1.964
h-cpe237	MCE	3.85	3.22	0.87	0.95	0.83	0.69	1.637	1.706

Figs. 4 and 5 show the response to the low-level DBE Corralitos ground motion (cls000) from the 1989 Loma Prieta earthquake. The response shown in Fig. 4(a) is the lateral roof drift

time history. The peak drift, 0.650% in the positive direction, occurs early in the response. The analytical prediction closely follows the experimental response. Fig. 4(b) shows the base overturning moment – roof drift hysteresis response. The flag-shaped loops are typical of self-centering systems. The analytical prediction is relatively close to the experimental response. Note the SC-CBF fully re-centers at the conclusion of the earthquake response. No structural damage was observed. Fig. 5 shows brace force time histories. The first story brace forces (Fig. 5(a)) reflect the base shear response. The fourth story brace forces (Fig. 5(b)) reflect both the roof-level inertial force and the PT force responses. Again, the analytical predictions follow the experimental responses.

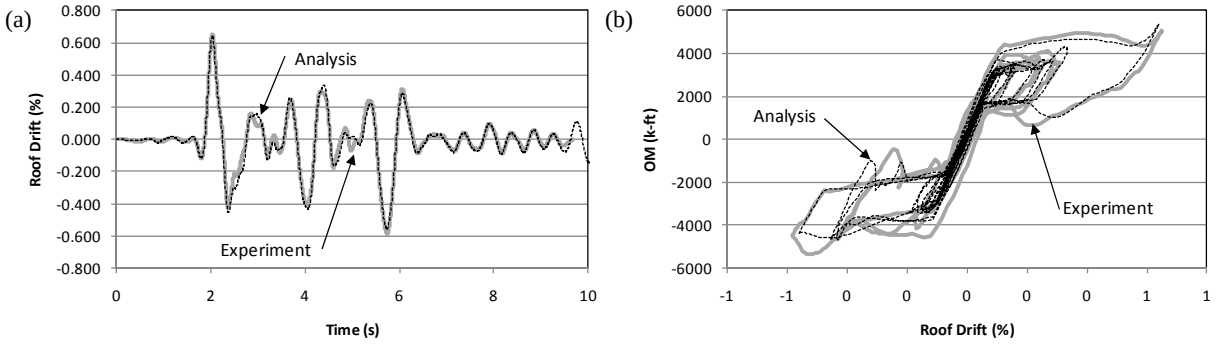

Figure 4. Response to DBE cls000: (a) roof drift time history; (b) overturning moment versus roof drift hysteresis loops. 1 k-ft = 1.356 kN-m.

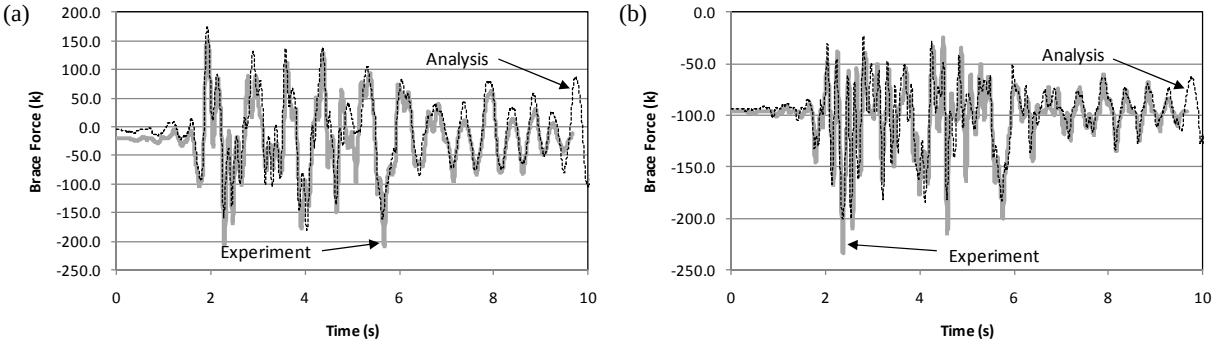

Figure 5. Response to DBE cls000: (a) first story south brace force time history; (b) fourth story south brace force time history. 1 k = 4.448 kN.

Figs. 6 and 7 show the response to the mean-plus-one-standard-deviation MCE Capitola ground motion (cap000) from the 1989 Loma Prieta earthquake. The lateral roof drift is shown in Fig. 6(a). The predicted peak response, the negative peak occurring at about 8 seconds of response, is 2.1%. The experimental peak response is 1.9%. Overall, the analytical prediction follows the experimental response. Fig. 6(b) shows the base overturning moment – roof drift hysteresis response. Due to the larger roof drift response under this record, the PT bars yielded slightly during the response. The plastic elongation of the PT bars reduced the prestress in the PT bars by 7%, which did not significantly affect the performance of the system. Fig. 6(a) shows that SC-CBF fully re-centers at the conclusion of the earthquake response. Fig. 7 shows the brace force response. Again, the analytical predictions generally follow the experimental responses

Summary and Conclusions

This paper presents the seismic performance of a newly developed concentrically-braced frame (CBF) system which has greater drift capacity before damage and which develops less permanent drift under seismic loading than a conventional CBF system. This self-centering CBF (SC-CBF) system is motivated by the goal of minimizing structural damage under seismic loading and is intended to provide significant non-linear drift capacity while limiting damage and residual drift.

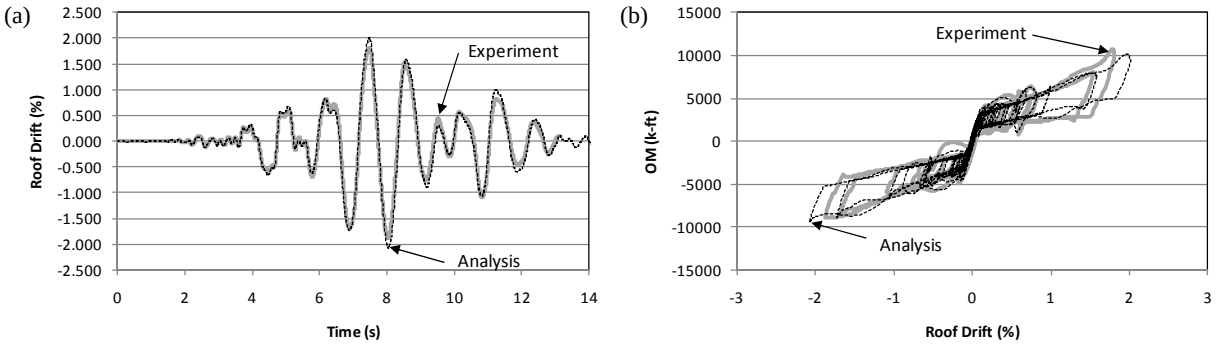

Figure 6. Response to MCE cap000: (a) roof drift time history; (b) overturning moment versus roof drift hysteresis loops. 1 k-ft = 1.356 kN-m.

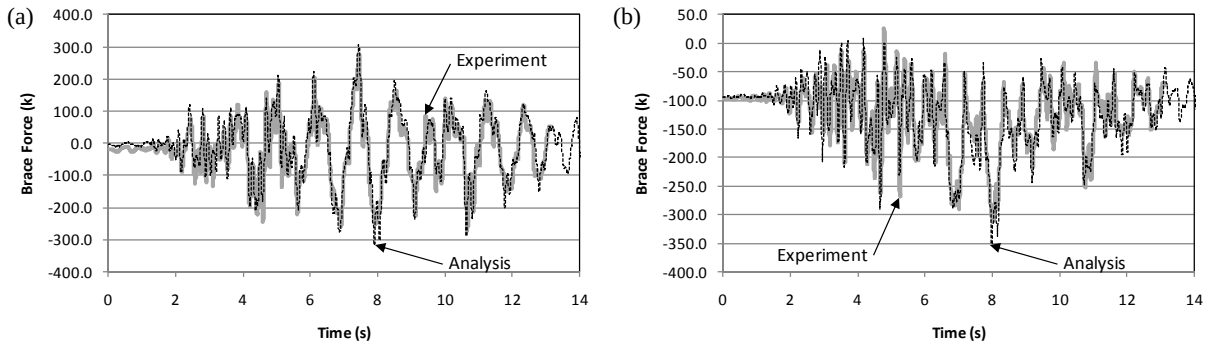

Figure 7. Response to MCE cap000: (a) first story south brace force time history; (b) fourth story south brace force time history. 1 k = 4.448 kN.

Important limit states and a performance-based seismic design (PBD) procedure for SC-CBFs were summarized. The performance objectives are immediate occupancy (IO) under the DBE and collapse prevention (CP) under the MCE. Analytical results for numerous earthquake ground motions and experimental results from several hybrid simulations on a large-scale test structure demonstrated that these performance objectives were reached. Analytical predictions were quite close to the experimental results, demonstrating the accuracy of the analytical model. Under DBE-level ground motions, no significant structural damage occurred, and under MCE-level ground motions only a small loss of prestress occurred. In all cases the SC-CBF re-centered after the seismic response.

Acknowledgments

This research was conducted at the NEES Real-Time Multi-Directional (RTMD) Earthquake Simulation Facility in the ATLSS Center at Lehigh University. This paper is based upon work supported by the National Science Foundation under Award No. CMS-0420974, within the George E. Brown, Jr. Network for Earthquake Engineering Simulation Research (NEESR) program and Award No. CMS-0402490 NEES Consortium Operation. Any opinions, findings, and conclusions or recommendations expressed in this material are those of the authors and do not necessarily reflect the views of the National Science Foundation.

References

Fahnestock, L.A., R. Sause, J.M. Ricles, and L.-W. Lu, 2003. Ductility Demands on Buckling Restrained Braced Frames Under Earthquake Loading, *Journal of Earthquake Engineering and Engineering Vibration* 2(2), 255-268.

Federal Emergency Management Agency (FEMA), 2003. *NEHRP Recommended Provisions for Seismic Regulations for New Buildings and Other Structures. Part 1 – Provisions and Part 2 – Commentary*, FEMA 450, Washington, D.C.

International Council (ICC), 2003. *International Building Code*, ICC, Falls Church, VA.

Kurama, Y., R. Sause, S. Pessiki, and L.-W. Lu, 2002. Seismic Response Evaluation of Unbonded Post-Tensioned Precast Walls, *ACI Structural Journal* 99(5), 641-651.

Mazzoni, S., F. McKenna, M.H. Scott, G.L. Fenves, et al. 2006. *Open System for Earthquake Engineering Simulation User Command-Language Manual*, Pacific Earthquake Engineering Research Center, University of California, Berkeley.

Perez, F.J., S. Pessiki, R. Sause, and L.-W. Lu, 2003. Lateral Load Tests of Unbonded Post-Tensioned Precast Concrete Walls, *Large-Scale Structural Testing*, ACI SP-211, 161-182.

Ricles, J.M., R. Sause, M. Garlock, and C. Zhao, 2001. Post-Tensioned Seismic-Resistant Connections for Steel Frames, *Journal of Structural Engineering* 127(2), 113-121.

Ricles, J.M., R. Sause, S.W. Peng, and L.-W. Lu, 2002. Experimental Evaluation of Earthquake Resistant Post-Tensioned Steel Connections, *Journal of Structural Engineering* 128(7), 850-859.

Roke, D., R. Sause, J. Ricles, C.-Y. Seo, and K.-S. Lee, 2006. Self-Centering Seismic-Resistant Steel Concentrically-Braced Frames, *Proceedings, Eighth U.S. National Conference on Earthquake Engineering*, San Francisco, April, EERI.

Roke, D., R. Sause, J.M. Ricles, and N. Gonner, 2009. Damage-Free Seismic-Resistant Self-Centering Steel Concentrically-Braced Frames, *STESSA 2009, Proceedings of the 6th International Conference on Behavior of Steel Structures in Seismic Areas*, Philadelphia, August.

Seo, C.-Y., 2005. Influence of Ground Motion Characteristics and Structural Parameters on Seismic Responses of SDOF Systems, *Ph.D. Thesis*, Lehigh University, Bethlehem, PA.